# Balun Modeling for Differential Amplifiers

Kun Chen, Zheng Liu, Xuelin Hong,  Ruinan Chang, and Weimin Sun

*Abstract*—**This work proposes an improved lumped element model for accurately characterizing transformer based baluns. The model can accurately describe balun behaviors for both differential and common modes. Lumped elements extraction from Y parameter is presented, and the relationship between the proposed model and the classic compact transformer model is derived. Numerical results will be presented to validate the accuracy of the proposed model.**

*Index Terms*—**balun modeling, transformer modeling, push-pull amplifiers, power amplifier (PA), compact model, differential mode, common mode, mutual inductance.**

## I. Introduction

TRANSFORMERS are important passive components which have various applications such as broadband impedance matching, power combining and dividing. They are found in many RF circuits and systems, and could be on-chip, on-die, or in package. Particularly, in the design of high performance differential (push-pull) power amplifiers (PAs), transformers serve as both inster-stage and output baluns. The use of transformer baluns enhances PA performance in the sense that the loadline is doubled for a given output power compared to single-ended PA, hence reducing loss due to a smaller impedance transformation ratio. Furthermore, it also offers significant common mode rejection, which will be beneficial for improving even order harmonic rejections.

Numerous models have been proposed to characterize transformers, like the compact model [1], Y-network model [2], transmission line model [3], frequency dependent transformer model [4], etc. However, little attention is paid to common mode modeling. In [5], a scalable model is proposed which takes into account both differential and common modes by adopting six mutual inductances, and physical and empirical based functions are used in determining the circuit parameters; however, one note for this model is that the phase imbalance prediction bandwidth is somewhat limited for multi-turn baluns.

The purpose of this paper is not an extensive scalable model that depicts different configurations for the balun; instead, the interest is in a simple and accurate lumped element model whose core elements (L, R, C) are explicitly extracted by its Y parameter which can be easily simulated by electromagnetic (EM) solver and measured by vector network analyzer (VNA) nowadays. In this way, one can then iterate the balun designs efficiently. Also, a new way of accounting for the common mode response is proposed, which models the common mode mutual inductance in an explicit and accurate manner.

The paper is organized as follows: In Section II, we will present the schematic and analysis of a transformer balun model, which is an extension of the classic mutual inductance

model. Particular for this core is an additional element which will be shown later to play a critical role in modeling common mode behavior. Section III will derive the formulae for extracting the model elements from the Y parameter. In Section IV, the differential, common and divider modes will be analyzed separately, where we will justify the addition of the extra element in the transformer core. Section V will discuss the relationship of the proposed transformer core model with the popular compact model that is based on ideal transformers and leakage and magnitization inductances. Section VI will discuss the physics and modeling of the common mode mutual inductance. And in Section VII, some straight-forward adaptations of the transformer core for more accurate modeling of actual transformer baluns, followed by numerical results in Section VIII. Finally, conclusions will be drawn in Section IX.

## II. Extended Balun Model
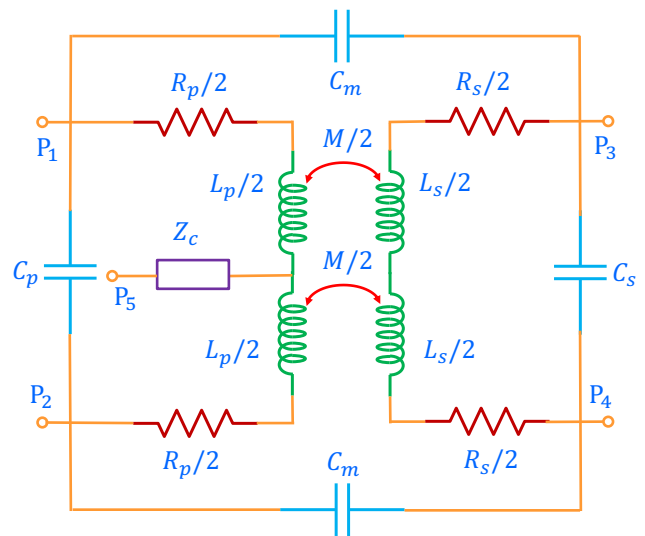


Fig. 1: Extended Balun Model

Fig. 1 shows the schematic of the proposed 5-port extended balun model. In this model, the primary inductor has series inductance $L_p$, series resistance $R_p$, and self-capacitance $C_p$, while the secondary inductor has $L_s$, $R_s$ and $C_s$. The primary and secondary inductors have a mutual inductance of $M$, and the mutual capacitances between primary and secondary inductor are denoted by $C_m$. For convenience, we have assumed that the inductors are equally split into two, and the polarity signs are on top side for all inductors unless otherwise specified, and parasitic capacitances other than $C_p$, $C_s$ and $C_m$ won't be considered until later sections. Compared to conventional balun model, the proposed model has an added impedance $Z_c$ at the center tap. In balun design, a proper center tap loading is usually desired for optimal

performance. But here we would consider $Z_c$ not as an external load, but as part of the balun model, and the value and meaning of it will be revealed later. In this model, mutual resistance is not included since it is usually negligible. Also, we only consider center tap at the primary, and it is trivial to generalize to the case with a center tap at the secondary.

Using Kirchhoff's current law and the definition of mutual inductance, one can find the following Y parameters of the balun model as

$$Y_{11} = j\omega(C_p + C_m) + \frac{Z_s}{Z_pZ_s + \omega^2 M^2} + \frac{1}{Z_p + 4Z_c} \quad (1)$$

$$Y_{12} = -j\omega C_p - \frac{Z_s}{Z_pZ_s + \omega^2 M^2} + \frac{1}{Z_p + 4Z_c} \quad (2)$$

$$Y_{13} = -j\omega C_m - \frac{j\omega M}{Z_pZ_s + \omega^2 M^2} \quad (3)$$

$$Y_{14} = \frac{j\omega M}{Z_pZ_s + \omega^2 M^2} \quad (4)$$

$$Y_{15} = -\frac{2}{Z_p + 4Z_c} \quad (5)$$

$$Y_{33} = j\omega(C_s + C_m) + \frac{Z_p}{Z_pZ_s + \omega^2 M^2} \quad (6)$$

$$Y_{34} = -j\omega C_s - \frac{Z_p}{Z_pZ_s + \omega^2 M^2} \quad (7)$$

$$Y_{35} = 0 \quad (8)$$

$$Y_{55} = \frac{4}{Z_p + 4Z_c} \quad (9)$$

where $Z_t = R_t + j\omega L_t, t \in \{p, s\}$. The rest of the Y parameters can be found by using reciprocity and symmetry of the network:

$$Y_{ij} = Y_{ji}, \ i \neq j \quad (10)$$
$$Y_{11} = Y_{22} \quad (11)$$
$$Y_{13} = Y_{24} \quad (12)$$
$$Y_{14} = Y_{23} \quad (13)$$
$$Y_{15} = Y_{25} \quad (14)$$
$$Y_{33} = Y_{44} \quad (15)$$
$$Y_{35} = Y_{45}. \quad (16)$$

### III. PARAMETER EXTRACTION AND FITTING

By extraction, here it refers to representing the lumped elements in the model as a function of the Y parameters; while by fitting, it means using simple empirical functions to extrapolate a wideband behavior from just a few frequency points. For the proposed model, we will regard all components as constant across frequencies except $R_p$ and $R_s$, because for most applications, the dependence of inductance and capacitance on frequency is very weak.

Looking at $Y_{11}$ and $Y_{12}$, one notices that

$$C_m = \frac{1}{j\omega}(Y_{11} + Y_{12} + Y_{15}) \quad (17)$$

From $Y_{34}$, $Y_{12}$, and $Y_{15}$, we get

$$Z_p = -j\omega M(Y_{34} + j\omega C_s)Y_{14}^{-1} \quad (18)$$

$$Z_s = -j\omega M(Y_{12} + \frac{1}{2}Y_{15} + j\omega C_p)Y_{14}^{-1} \quad (19)$$

Plugging Eq. (18-19) into Eq. (4) and simplifying, we yield

$$M = \frac{j}{\omega[Y_{14} - Y_{14}^{-1}(Y_{12} + \frac{1}{2}Y_{15} + j\omega C_p)(Y_{34} + j\omega C_s)]}. \quad (20)$$

With $Z_p$, $Z_s$ and $M$, the coupling factor $K$ and turn ratio $T$ are defined as

$$K = M/\sqrt{L_pL_s} \quad (21)$$

$$T = \sqrt{L_s/L_p}. \quad (22)$$

For $Z_c$, one can easily write that

$$Z_c = \frac{1}{Y_{55}} - \frac{1}{4}Z_p \quad (23)$$

In the above extraction, $Z_p$, $Z_s$, $Z_c$ and $M$ depend on $C_p$ and $C_s$, which are usually much smaller than $C_m$, and only play a noticeable role at very high frequencies. In most cases, we can directly put $C_p = C_s = 0$ and still maintain good accuracy. However, instead of regarding $C_p$ and $C_s$ as nil, it makes more sense to get an approximate expression for them.

One can write that

$$Y_{12} - \frac{1}{4}Y_{55} = -j\omega C_p - \frac{Z_s}{Z_pZ_s + \omega^2 M^2}. \quad (24)$$

For $Z_t$, $t \in \{p, s\}$, using Taylor expansion for the resistive part $R_t$, we have

$$Z_t \approx R_{t,0} + \omega(R_{t,\omega,0} + jL_t) \quad (25)$$

where $R_{t,0} = R_t|_{\omega=0}$, $R_{t,\omega,0} = \partial R_t/\partial\omega|_{\omega=0}$. When $R_{t,0} \ll \omega|R_{t,\omega,0} + jL_t|$, which is the case when the quality factor $Q_t$ of the inductor is not very small, or when the frequency is high enough, we have, from Eq. (24),

$$C_p \approx -\frac{\partial\omega(4Y_{12} - Y_{55})}{8j\omega\partial\omega}. \quad (26)$$

Note that in the above, the right hand side is a complex number, while the left hand side should be real. The interpretation is that the imaginary part of the right hand side is much smaller than the real part and shall be ignored. This convention is assumed through this work.

Similarly, one obtains

$$C_s \approx -\frac{\partial\omega(2Y_{34} + Y_{35} + Y_{45})}{4j\omega\partial\omega} \quad (27)$$

where $Y_{35}$ and $Y_{45}$ are added to make it more numerically robust. As mentioned previously, only the resistance $R_p$ and $R_s$ have strong frequency dependence, which is mostly due to skin effect and proximity effect. The resistance model in [6] can be adopted:

$$R_t = R_{t,dc}(\xi_t \coth\xi_t)' \cdot (1 + r_{t,rf}\frac{(f/f_{0t})^2}{1 + (f/f_{0t})^2}) \quad (28)$$

where $(\cdot)'$ means taking the real part, and $\xi_t = (1 + j)\frac{t_t}{2\delta}$ with $\delta$ being the skin depth, and $t_t$ the thickness of the metal, while $r_{t,rf}$ is a constant determined by geometry and technology, and $f_{0t}$ is a frequency factor which can be determined by some fitting. From this model, the RF part of $R_t$ behaves like $\sim f^2$ at low frequency, while $\sim \sqrt{f}$ at high frequency.

## IV. DIFFERENTIAL, COMMON AND DIVIDER MODE

In push-pull amplifier design, the balun can serve as a power divider or combiner. When employed at the output stage as a combiner, it's two inputs can be decomposed into differential and common modes. When operating as a combiner, we assume Port 1 and 2 are inputs, Port 3 is output, while Port 4 is grounded; for the case of divider, Port 3 is the input, and Port 1 and 2 the output, while Port 4 remains grounded. And in general, for Port $i$, the excitation, if any, is a voltage source $S_i$, and the source or load impedance is $Z_i = R_i + jX_i$.

By definition of the Y parameter, we have

$$I_i = \sum_j Y_{ij} V_j \tag{29}$$

where $5 \geq i, j \in \mathcal{N}_+$, and $I_i$ is assumed to flow into Port $i$. In addition, the constraints from the loading and sources give the following:

$$S_k - V_k = I_k Z_k, \ k \in \{1, 2, 3\} \tag{30}$$
$$V_4 = 0 \tag{31}$$
$$V_5 = -I_5 Z_5. \tag{32}$$

The above equations can be solved for $I_i$ and $V_i$, which can then be used to calculate input impedance and insertion loss. The expressions for the general case are very involved, and some special cases will be examined to gain some insights.

### A. Differential Mode

For differential mode, we set $S_1 = -S_2 = 1V$, $S_3 = 0$, and assume $C_p = C_s = C_m = 0$ for simplicity. The input impedance at Port 1 and 2 can be found as

$$Z_{in1,diff} = Z_{in2,diff} = \frac{1}{2}\left(Z_p + \frac{\omega^2 M^2}{Z_3 + Z_s}\right) \tag{33}$$

and the power gain (or insertion loss with input mismatch removed) is

$$G_{p,diff} = \frac{R_3}{R_3 + R_s + T_{sp}^2 R_p} \tag{34}$$

with $T_{sp} = \frac{|Z_3 + Z_s|}{\omega M}$. It is worth to note that $Z_{in1,diff} = Z_{in2,diff}$ indicates the two input impedances are balanced, which is true as long as $C_m = 0$. It is not difficult to show that the presence of $C_p$ and $C_s$ doesn't affect the balance of the two input impedances, which is neglected for conciseness.

### B. Common Mode

In this case, we only assume $C_m = 0$, and set $S_1 = S_2 = 1V$, $S_3 = 0$. The common mode input impedance is found to be

$$Z_{in1,comm} = Z_{in2,comm} = \frac{1}{2}Z_p + 2(Z_5 + Z_c). \tag{35}$$

Because $C_m = 0$, the common mode is completely rejected and the power gain of common mode is 0. However, if $C_m \neq 0$, we will have only finite common mode rejection, and the input impedances won't be balanced either. One thing to notice is that the common mode signal sees an impedance that is simply half of $Z_p$ plus two times of $Z_5 + Z_c$, while the differential mode signal doesn't see $Z_5 + Z_c$ at all,

which indicates $Z_c$ can be used to manipulate the common mode behavior of the model without significantly disturbing the differential mode. Also, power gain is considered here because in power amplifier design, it is more related to the power efficiency.

### C. Divider Mode

Assuming $C_p = C_s = C_m = 0$, $Z_1 = Z_2 = Z_{div} = R_{div} + jX_{div}$, and requiring $S_1 = S_2 = 0$, $S_3 = 1V$, The input impedance of divider mode can be shown as

$$Z_{in3,div} = Z_s + \frac{\omega^2 M^2}{Z_p + 2Z_{div}} \tag{36}$$

and the power gain (with the two output power combined) is

$$G_{p,div} = \frac{2R_{div}}{2R_{div} + R_p + T_{ps}^2 R_s} \tag{37}$$

where $T_{sp} = \frac{|2Z_{div} + Z_p|}{\omega M}$.

## V. RELATIONSHIP WITH IDEAL TRANSFORMER BASED MODEL
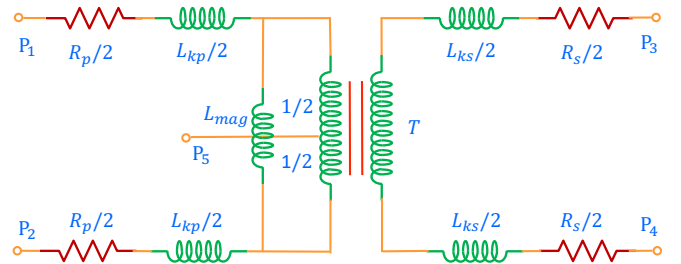


Fig. 2: Compact Balun Model Based on Ideal Transformers

Figure 2 shows a balun core model based on an ideal transformer [1]. Here we neglect all the parasitic capacitances, and shall compare it with the proposed extended balun model in Fig. 1 with capacitances removed. In this model, the leakage and magnetization inductances are given as

$$L_{kp} = (1 - K)L_p \tag{38}$$
$$L_{ks} = (1 - K)L_s \tag{39}$$
$$L_{mag} = KL_p. \tag{40}$$

The Y parameter of this 5-port network can be derived, which is found to be identical to that of the proposed model in Fig. 1 with $Z_c = -\frac{K}{4}j\omega L_p$ and $C_p = C_s = C_m = 0$. This equivalence under a condition involving $Z_c$ infers that there is some physical meaning that can be sought for regarding $Z_c$. Also, due to the observation in simulation the insufficiency of the model in Fig. 2 to capture common mode behavior accurately, $-\frac{K}{4}j\omega L_p$ may not be the right value for $Z_c$.

## VI. COMMON MODE MUTUAL INDUCTANCE

When the balun is driven by common mode signals at Port 1 and 2, the current flow is illustrated in Fig. 3. Note that the two currents will combine and flow into Port 5. This simplified model, neglecting capacitive coupling, indicates
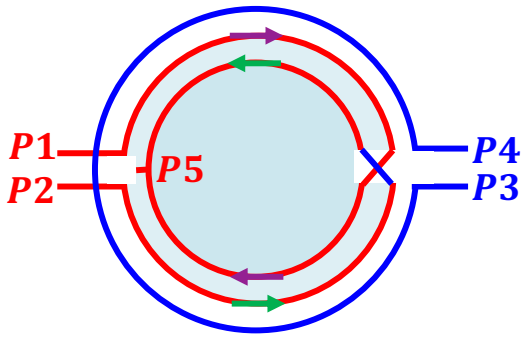
Fig. 3: Illustration of Common Mode Mutual Inductance
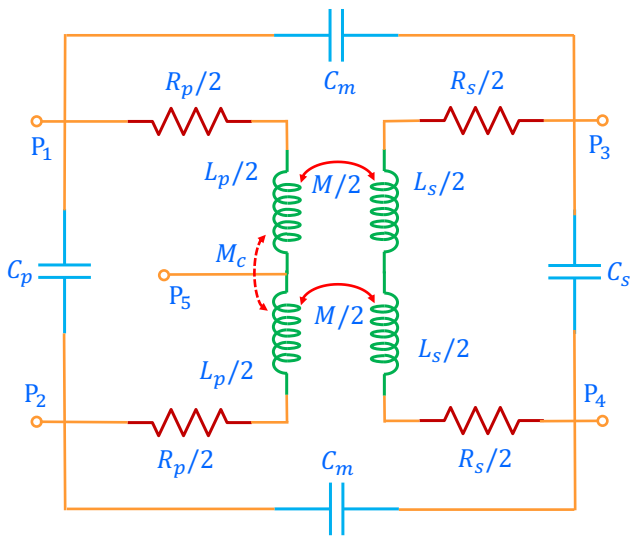


Fig. 4: Balun Model with Both Differential and Common Mode Mutual Inductance



(a) Mutual Inductance Model  (b) T-network Model
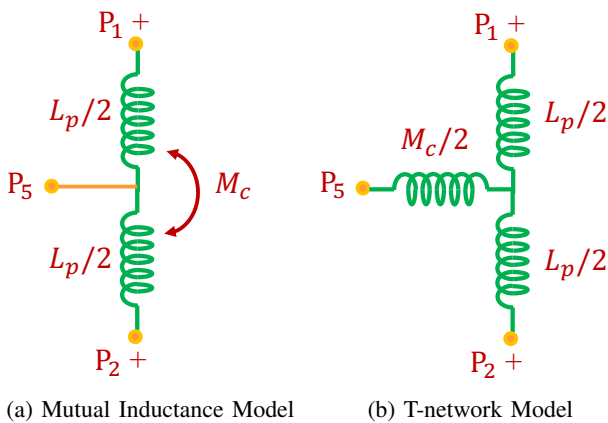
Fig. 5: Common Mode Equivalent Circuit

some negative mutual inductance between the two halves of the primary inductor when it has multiple turns. Also, without mutual capacitance, due to the symmetry of the system, there is no net current on the secondary inductor. The mutual inductance within the primary inductor can be modeled by Fig. 5 (a), where "+" on top and bottom means the two excitations are in phase, and $M_c$ is the common mode mutual inductance. Since $M$ is for differential mode mutual

inductance, while $M_c$ for common mode mutual inductance, in the idealized case of having no mutual capacitance, the differential mode signals should not see $M_c$, while $M$ should also be invisible to common mode signals. However, a direct addition of $M_c$ through mutual inductance mechanism as in Fig. 4 (polarity signs lie where the arrows point) will make the two modes entangled and unable to decouple, which is actually against the physics. To reconcile this contradiction, we just need to resort to the proposed model in Fig. 1 and let $Z_c = \frac{1}{2}j\omega M_c$, as we can show the T-network model in Fig. 5(b) is equivalent to 5(a) for common mode excitations. As we've shown in Eq. (33) and (35), in the absence of mutual capacitance, the differential mode is independent of $Z_c$, while the common mode won't see $M$. By letting $Z_c = \frac{1}{2}j\omega M_c$, the extended balun model will be able to model both differential and common mode.
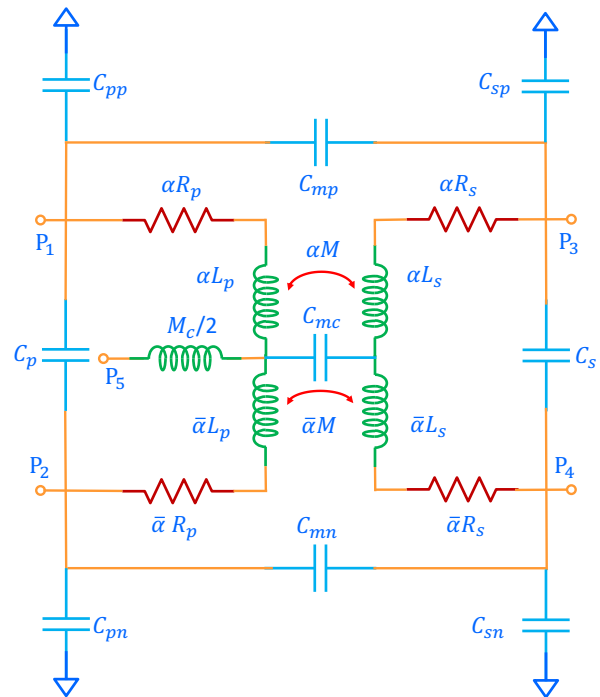


Fig. 6: Extended Balun Model with Asymmetry and More Parasitic Capacitances

## VII. Adaptation for Model Fitting

The discussions so far are restricted to a symmetric balun model. However, in practice, one may find it difficult to lay such a symmetric balun out. Also, there will always be some amount of parasitic capacitance/resistance to ground. Fig. 6 shows one example of the model, where $\bar{\alpha} = 1 - \alpha$ and the primary and secondary inductors are not equally split. The mutual capacitance is distributed into $C_{mp}$, $C_{mn}$, and $C_{mc}$, while the shunt capacitances to ground $C_{pp}$, $C_{pn}$, $C_{sp}$, and $C_{sn}$ are added. In highly lossy substrate, one may also add shunt resistance to ground, but here we assume not such a case. It should be pointed out that introducing shunt parasitic capacitances and distributing mutual capacitances can make the model more accurate in a wider bandwidth, but the analytic extraction of those capacitances becomes more involved and it may be enough in practice resorting to fitting to decide their values.
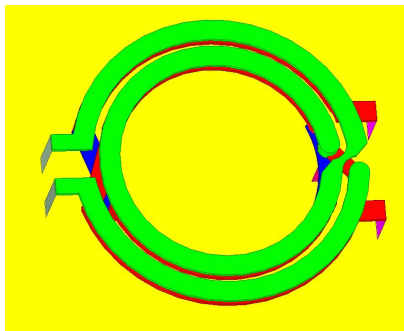
Fig. 7: Double Turn Balun

## VIII. NUMERICAL RESULTS

Fig. 7 shows a 5-port circular balun HFSS model, which has two turns for both the primary and secondary coils. The thickness of metals is 20um, while the separation between adjacent layers is 30um. For both coils, the inner diameter is 1mm, the trace width is 100um, while the gap between neighboring turns is 35um. The balun is placed such that bottom layer metal is lifted 200um from the PEC ground plane. Here we assume that the substrate is with a relative dielectric constant of 4, while the metal is copper with a conductivity of $5.8e7$S/m. We also assume that this balun is operating at 1GHz, but its behavior up to 5GHz will be examined. It should be noted that, for such a passive structure, HFSS can predict very well the actual performance, so we will use the EM solver's results as a reference to validate the proposed balun mode.

With the S parameter from HFSS simulation, we first extracted the key balun parameters using the formulae proposed in Sec. II. Then a brute force ADS optimization is performed to fit the HFSS S parameter with the extended baun model. The fitting seeks for a set of optimized parameters such that $|S_{ij} - \tilde{S}_{ij}| < \epsilon$ for a specified tolerance $\epsilon$, where $S_{ij}$ and $\tilde{S}_{ij}$ are the S parameters for the HFSS model and the lumped model respectively. In the S parameter simulation, the reference impedance is chosen as $10\Omega$ instead of $50\Omega$ in order to see a larger impedance contour on the smith chart for better resolution. Another consideration is that the loadline of a power amplifier for LTE is closer to $10\Omega$ than $50\Omega$.

Table I is a summary of the key balun parameters from extraction and fitting, with dimensions nH for inductances and $\Omega$ for resistances. Since we have assumed weak frequency dependence of the inductances, the extracted inductances can be from DC, but instead they were from a very low frequency (100MHz) due to HFSS's low frequency breakdown leading to inaccurate results when the frequency is approaching DC. For the resistances, the values are from 1GHz, the operating frequency. From this table, we can see that the extracted parameters match very well with the fitted parameters. We also notice the common mode mutual inductance of 1.8nH, which is not trivial as to be neglected.

In order to validate the proposed model for all modes, we can just compare the S parameters directly with HFSS simulation. The S parameters from HFSS simulation and extended balun model fitting are overlaid in Fig. 8 and 9. In the fitting, only the resistances are frequency dependent, while all other components are constants. Reciprocity and symmetry of the model are invoked and only necessary S pa-

rameter components are shown. We can see that, up to 5GHz, good agreement for impedance, reflection and transmission is achieved between HFSS simulation and the extended balun model. This indicates that the extended balun model has captured the physics accurately within this frequency range.

TABLE I: Balun Parameters

| Parameter | $L_p$ | $R_p$ | $L_s$ | $R_s$ | $M$ | $M_c$ | $\alpha$ |
|-----------|-------|-------|-------|-------|-----|-------|----------|
| Extracted | 5.2 | 0.52 | 5.6 | 0.59 | 4.0 | -1.8 | 0.5 |
| Fitted | 5.2 | 0.49 | 5.5 | 0.57 | 4.1 | -1.8 | 0.5 |
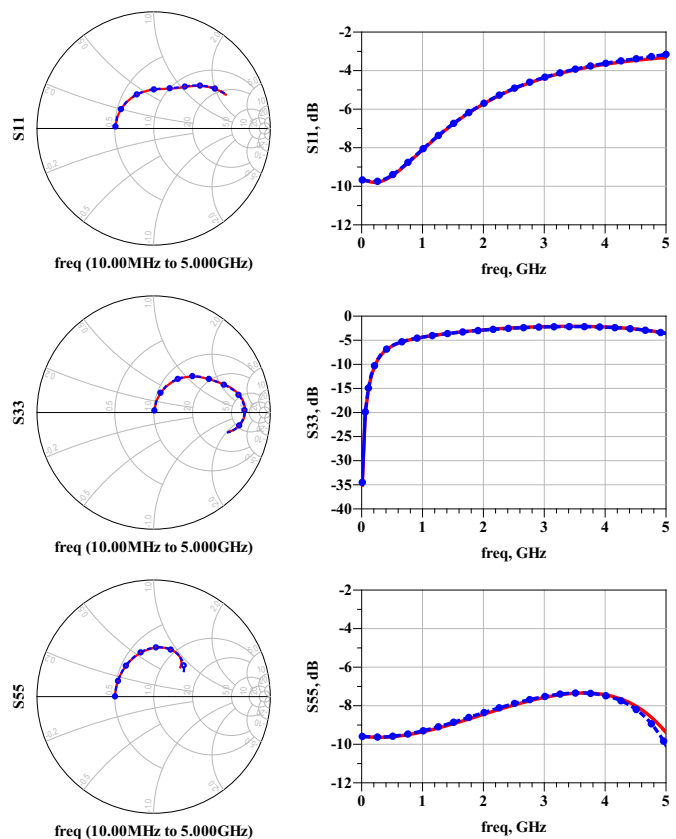


Fig. 8: Reflection. HFSS (solid) v.s. lumped (dotted).

## IX. CONCLUSIONS

This paper proposed an extended balun model which properly accounts for both differential and common mode mutual inductances. The model's lumped elements are first derived from its Y parameters, and then the three different modes, differential, common and divider mode, are inspected when no parasitic capacitances are present. In these cases, one notices that the differential mode doesn't see the center tap load, while the common mode does. By comparing with the ideal transformer based balun model, we found the equivalence between the two models when the center tap is loaded with $-\frac{K}{4}j\omega L_p$. Further, common mode mutual inductance is discussed from both a physical and circuit point of view, and an equivalent T-network is hence proposed to accommodate the physics without contradiction, which is incorporated in the extended balun model. Then, some straightforward adaptations are made to account for more parasitic capacitances and asymmetry to make the model
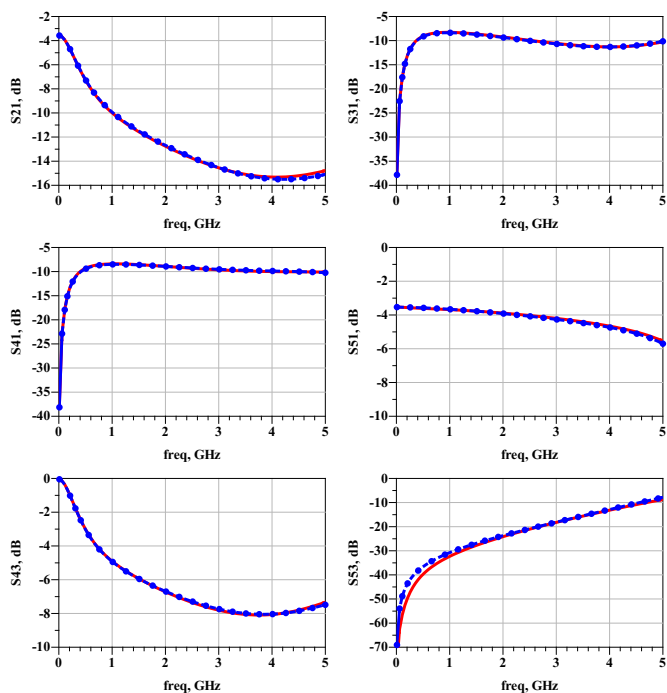
Fig. 9: Transmission. HFSS (solid) v.s. lumped (dotted).

more accurate. Finally, the accuracy of the proposed model is confirmed by numerical results. The model is considered in the context of push-pull amplifiers, and can be used to aid amplifier designs.

## REFERENCES

[1] J. R. Long, "Monolithic transformers for silicon RF IC design," *IEEE Journal of Solid-State Circuits*, vol. 35, no. 9, pp. 1368-1382, Sept. 2000.

[2] Jonguk Kim, Hyun-Tai Kim, Kwi-Soo Kim, Jong-Sik Lim and Dal Ahn, "An equivalent circuit model for multi-port networks," *2007 European Microwave Conference*, Munich, 2007, pp. 901-904.

[3] D. Chowdhury, P. Reynaert and A. M. Niknejad, "Design Considerations for 60 GHz Transformer-Coupled CMOS Power Amplifiers," *IEEE Journal of Solid-State Circuits*, vol. 44, no. 10, pp. 2733-2744, Oct. 2009.

[4] Y. Mayevskiy, A. Watson, P. Francis, Kyuwoon Hwang and A. Weisshaar, "A new compact model for monolithic transformers in silicon-based RFICs," *IEEE Microwave and Wireless Components Letters*, vol. 15, no. 6, pp. 419-421, June 2005.

[5] L. F. Tiemeijer, R. M. T. Pijper, C. Andrei and E. Grenados, "Analysis, Design, Modeling, and Characterization of Low-Loss Scalable On-Chip Transformers," *IEEE Transactions on Microwave Theory and Techniques*, vol. 61, no. 7, pp. 2545-2557, July 2013.

[6] H. Gan, "On-chip transformer modeling, characterization and applications in power and low noise amplifiers," *PhD thesis*, Stanford University, March 2006.